AIP | Applied Physics Letters

C-scan photoacoustic microscopy for invivo imaging of Drosophila pupae

Lei Xi, Lei Zhou, and Huabei Jiang

Citation: Appl. Phys. Lett. **101**, 013702 (2012); doi: 10.1063/1.4732797
View online: http://dx.doi.org/10.1063/1.4732797
View Table of Contents: http://apl.aip.org/resource/1/APPLAB/v101/i1
Published by the American Institute of Physics.

C-scan photoacoustic microscopy for *in vivo* imaging of *Drosophila* pupae

Lei Xi,[1] Lei Zhou,[2] and Huabei Jiang[1,a)]
[1]*Department of Biomedical Engineering, University of Florida, Gainesville, Florida 32611, USA*
[2]*Department of Molecular Genetics and Microbiology, University of Florida, Gainesville, Florida 32611, USA*

(Received 17 May 2012; accepted 11 June 2012; published online 2 July 2012)

In this study, C-scan based high resolution photoacoustic microscopy (CPAM) is devised and used to *in vivo* image the DsRed-expressing cells in the central nervous system (CNS) of *Drosophila* pupae. The quality of out-of-focus images was improved significantly from both the phantom and *in vivo* experiments. Organs containing DsRed-expressing cells in *Drosophila* pupae can be imaged using our CPAM and agreed well with the histological sections. This technology allows rapid imaging and monitoring of organismal development in mesoscopic-scale animals as well as the generation of a detailed atlas of CNS development in the pupal stage. © *2012 American Institute of Physics*. [http://dx.doi.org/10.1063/1.4732797]

Animals such as *Drosophila*, zebrafish, and *Xenopus laevis* are widely used as models for studying mesoscopic-scale events. As such, there is a rapidly growing interest in developing optical modalities for *in vivo* imaging such mesoscopic-scale animals. Currently, at the organ and organism level, most high resolution optical imaging modalities such as epifluorescence microscopy, fluorescent confocal microscopy, and two-photon microscopy are not suitable for visualizing objects located $\geq$1 mm deep within tissue due to the limitation of one optical transport mean-free-path ($\sim$1 mm) in high scattering tissues.[1–3] To overcome this limitation, Vinegoni *et al.*[4] reported *in vivo* fluorescent tomographic imaging of green fluorescent protein (GFP)-expressing cells inside *Drosophila* pupae based on Fermi simplification to the Fokker-Planck solution of photon transport theory. However, the theoretical model used is suitable only for strongly forward-scattering regimes and hence a polarizer had to be used to reject highly diffusive photons. Tan *et al.*[5] showed the possibility of *in vivo* monitoring DsRed-expressing cells in *Drosophila* pupae via radiative transfer equation (RTE) based fluorescence tomographic imaging without mathematical simplifications. Razansky *et al.*[6] employed conventional circular-scan based photoacoustic tomography (PAT) to *in vivo* image eGFP-expressing organs in *Drosophila* pupae and mCherry fluorecent proteins in zebrafish. It is noted that these fluorescence and photoacoustic tomographic approaches do not provide adequate spatial resolution to visualize the microscopic events associated with the mesoscopic-scale animals.[4–6]

Photoacoustic microscopy (PAM) has demonstrated high resolution ability for *in vivo* applications in vascular biology, ophthalmology, dermatology, and gastroenterology due to the use of high-frequency ($\geq$30 MHz) focused transducer.[7–14] It is noted that these applications are either limited to the objects with high optical absorption or subject to the utilization of high power illumination. Without signal averaging, the signal-to-noise ratio (SNR) for low absorption targets or under the condition of low power illumination will not be able to produce an usable image. Another limitation associated with the conventional PAM is its limited depth of focus for the focused high-frequency transducer used, which generates deteriorated images for out-of-focus planes. Li *et al.*[15] showed the improvement of out-of-focus resolution through employing a virtual-detector based synthetic-aperture focusing technique (SAFT) for high absorbing objects such as blood vessels. For most low absorbing objects existing in biological tissue, signal averaging is needed using the SAFT method. It is known that the use of low power illumination is a required condition for imaging mesoscopic-scale animals, since high power illumination will either interrupt the biological development of interest or damage the animals. Here, we explore a PAM approach based on axial scanning or C-scan instead of signal averaging to improve the out-of-focus resolution for low absorbing objects under the condition of low power illumination.

In our C-scan based high resolution photoacoustic microscopy (CPAM) system shown in Fig. 1(a), a 532 nm pulsed laser was used to generate a short-pulsed laser beam with 6 ns duration at 10 Hz repetition rate. Then, the laser beam was split into two sub-beams and each of sub-beams was coupled into an optic fiber bundle. The two optic fiber bundles were fixed in opposite positions to produce a homogenous volume illumination through the object. Induced photoacoustic waves were received by a focused high-frequency ultrasound transducer (50 MHz, 3 mm aperture, and 6 mm focal length). The imaging probe consisting of the transducer and optic fiber bundles was mounted on a three-dimensional (3D) moving stage. This system can provide a lateral resolution of 61 μm on the focal point (Fig. 1(b)) and an axial resolution of 15 μm.

The pupa was fixed on a holder with its long side parallel to Y axis (Fig. 1(a)). The scanning step was set to be 25.4 μm along X and Y axis and 50 μm along Z axis. During the *in vivo* experiments, low laser energy (0.5 mJ/cm^2) was used to ensure uninterrupted biology development of the pupa. We noticed that all the pupae imaged developed into fruit flies with this laser energy.

In conventional PAM, photoacoustic signal is collected at each location of transducer, resulting in one-dimension (1D) depth-resolved image. A 3D image is produced by scanning the ultrasound transducer in X-Y plane. For low optical

a)Author to whom correspondence should be addressed. Electronic mail: hjiang@bme.ufl.edu.

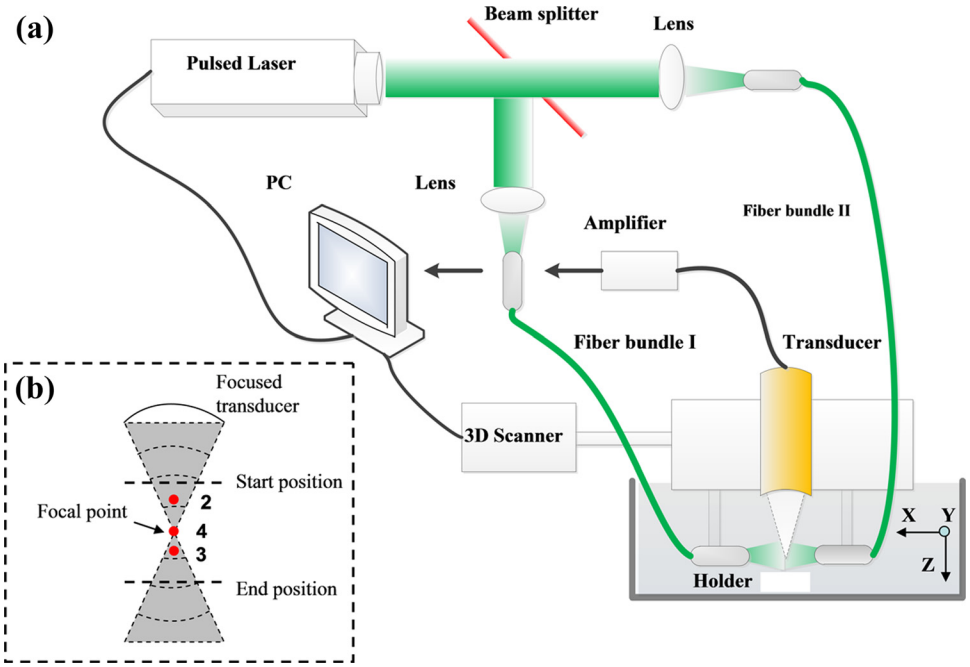

FIG. 1. (a) Schematic of the photoacoustic system. (b) C-scan PAM concept. The start and end positions are typically 0.5 mm away from the focal point.

absorbing objects, the photoacoustic signals need to be averaged at each transducer location to increase the SNR. In our CPAM, for each 1D depth-resolved image, the focal point of the transducer is scanned along Z axis (i.e., axial scanning from the start position to the end position in Fig. 1(b)) and the signals collected at all the points along Z axis are used to reconstruct a 1D image as follows:

$$P(t) = \frac{\sum_{n}^{j=1} p(j, t - (j-1) \times t_0)}{n}, \tag{1}$$

where $p(j,t)$ is the signal received at the j the focal point during the axial-scanning, t_0 is the calculated time of acoustic wave propagation for one scanning step along Z axis, and n is the total scanning steps used for the axial-scanning. In each axial scanning, t_0 is defined as

$$t_0 = \triangle L / V_c, \tag{2}$$

where $\triangle L$ represents the distance of one scanning step (50 μm in our study) and V_c is the sound velocity in water (1.5 mm/μs). Similar to the B-mode ultrasound image formation, the reconstructed time-resolved signal $P(t)$ is then used to form a 1D photoacoustic microscopic image as a function of z coordinate

$$I(z) = P(t) \times V_c. \tag{3}$$

The image reconstruction method described above was validated through phantom experiments. In these experiments, a

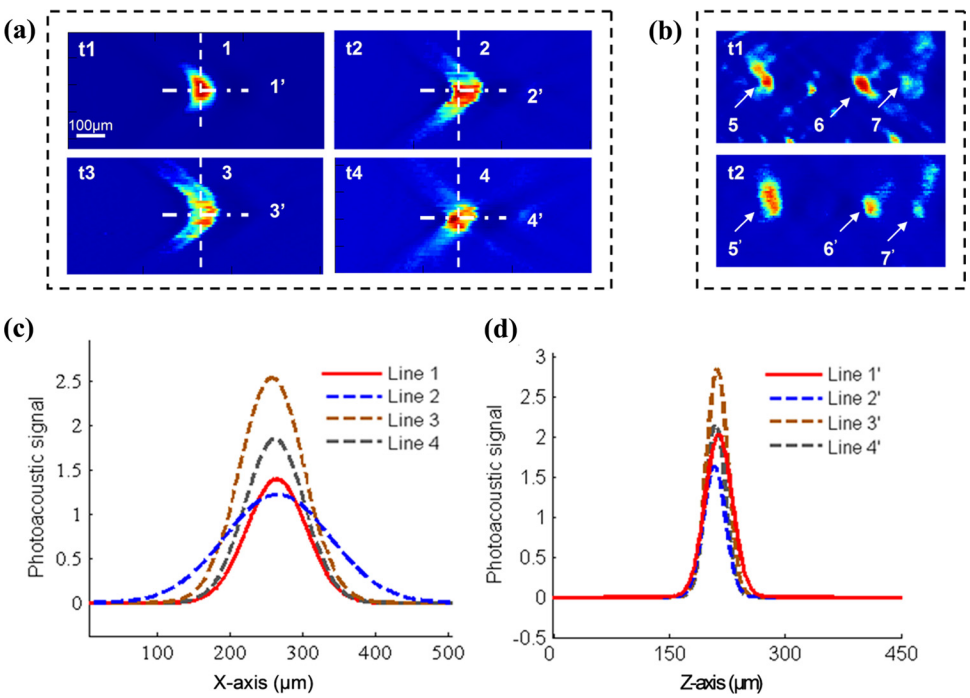

FIG. 2. (a). The image of hair by C-scan PAM (t1), and the image of hair located at different positions by conventional PAM (t2, t3, and t4). (b). *In vivo* pupa images by C-scan PAM (t2) and by conventional PAM (t1). (c). Lateral profiles for the images shown in (a). (d). Axial profiles for the images shown in (a).

TABLE I. Comparison of the target size measured by CPAM and actual value.

Line No.	Distance form the focal point (μm)	Actual size (μm)	Recovered lateral size (μm)	Recovered axial size (μm)	Error (lateral)
1	NA	98	105	99	6.1%
2	450	98	170	99	73.5%
3	300	98	135	99	37.6%
4	0	98	99	99	1.0%

human hair was embedded in a standard agar-powder (2%) solidified human tissue mimicking phantom, consisting of Intralipid as the scatterer and India ink as the absorber. The absorption coefficient of the phantom was 0.007 mm^{-1} and the reduced scattering coefficient was 1.0 mm^{-1}. Due to the high absorption of hair, we used low-energy illumination of 0.1 mJ/cm^2 for these experiments.

The image probe was scanned for 25 steps with a step size of 50 μm along Z axis from starting position to ending position (Fig. 1(b)) and the raw data collected from all the axial-scanning points were used to produce an 1D image. Each 2D image contained 50 1D images. Fig. 2(a) (t1, upper left) shows the reconstructed image using the axial-scanning method, while Fig. 2(a) (t2, t3, and t4) show the images recovered by averaging the signals 25 times without the use of the axial-scanning when the hair was in positions 2, 3, and 4, respectively (Fig. 1(b)). Transverse and axial profiles along the dashed lines 1, 1′, 2, 2′, 3, 3′, 4, and 4′ in Fig. 2(a) are given in Figs. 2(c) and 2(d) after Hilbert transform and Gaussian fitting of the raw data. Quantitative information was extracted from the profiles shown in Figs. 2(c) and 2(d) and summarized in Table I.

From Table I, we see that t1 image provides accurate quantitatively reconstructed transverse hair diameter with an error of 6.1% compared to the true value. t2 and t3 images show a large error of 73.5% and 37.6%. t4 image gives the most accurate transverse size of target with an error of less than 1% because the hair was placed right at the focal point of transducer. For axially imaged size, accurate results with an error of less than 1% were obtained for all the four cases, since the axial resolution (15 μm) was determined by the frequency and bandwidth of the transducer regardless of the target positions.

For embryos and larvae, the morphogenesis of the central nervous system (CNS) can be monitored with conventional fluorescence microscope (FM). However, the signal is completely blocked following the formation of the pupal case using conventional FM. The fragileness of the pupal tissue coupled with the hardness of the pupal case makes it extremely difficult to dissect the animal without harming the normal developmental process. With the CPAM technology, it is feasible to *in vivo* observe the development and morphogenesis of the CNS in the pupal stage.

Drosophila melanogester of the genotype elav-Gal4; UAS-DsRed were grown in standard media in 25 °C. Within 24 h following pupation, pupae were removed from the vial. A small hole was made at the posterior as well as the anterior end of the pupal case with a fine tungsten needle under a dissection scope. The punctuated pupae were quickly immersed in 1 ml of 4% paraformaldehyde in PBS (phosphate buffered saline) in a 1.5 ml eppendorf tube. The tube was let rotate in room temperature for 24 h. Certain histological sections were performed by frozen sectioning machine and imaged by fluorescence optical microscopy system.

The *in vivo* PAM experiments were conducted following the same procedure as the phantom experiments except for the use of increased laser energy (0.5 mJ/cm^2). The pupa was fixed in a small tube filled with transparent agar powder solidified material as shown in Fig. 3(a). The scanning took 2 min for each 2D PAM image.

Fig. 2(b) presents the PAM images of pupa by C-scan PAM (t2) and by conventional PAM (t1). The DsRed-expressing cells indicated by arrow 5 in t1 are more accurate than the same part indicated by 5′ in t2 because the size is smaller in t1 than that in t2. In this case, these DsRed-expressing cells were close to the focal point, so that we could obtain the highest resolution and best reconstructed size. For other DsRed-expressing cells indicated by 6, 6′, 7, and 7′, we also see that the image quality with C-scan is notably higher. And the background of t2 is obviously cleaner than t1.

Fig. 3(a) shows the position/section corresponding to the CPAM/FM slices presented in Figs. 3(b)–3(e) where the top row shows the *in vivo* photoacoustic images and the bottom row gives fluorescence microscopic images of the corresponding histological sections. Major features are clearly identifiable in CPAM images and agree well with the corresponding histological sections.

We have presented an improved high-resolution PAM approach for *in vivo* monitoring DsRed-expressing cells/organs in *Drosophila* pupae. This technique allows rapid and

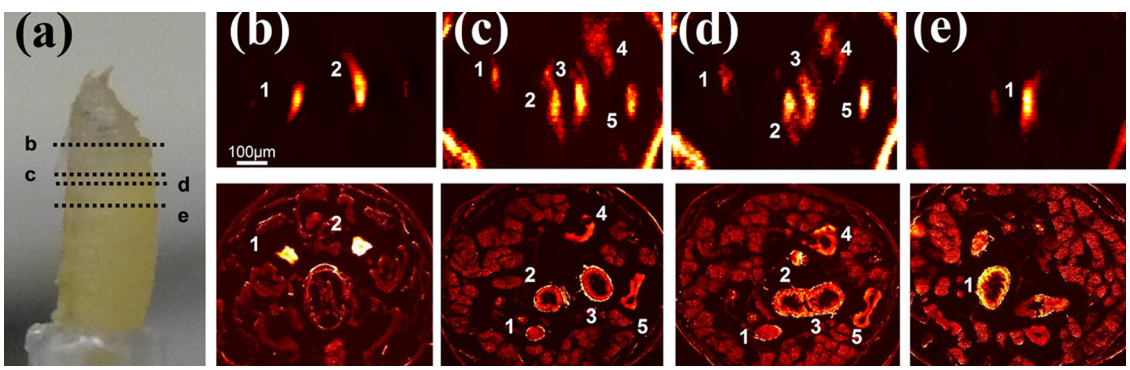

FIG. 3. *In vivo* CPAM images (top row. (b)-(e)), and fluorescence microscopic images of histologic sections (bottom row (b)-(e)).

continuous imaging of organism development in high resolution. Our method can be implemented in a straight forward way to study other mesoscopic-scale animals such as zebrafish and larvae of frogs. We note that photoacoustic imaging has limitations for imaging mesoscopic tissues without labeling. For example, we may need to combine our CPAM with other modalities such as optical coherence tomography (OCT) or high-resolution ultrasound microscopy to provide complementary fine structural information. For our CPAM, improvements are needed especially with respect to the wavelengths of laser and data acquisition time. In this study, only 532 nm-pulsed laser with low repetition rate (10 Hz) was used. In future studies, high-speed tunable near-infrared pulsed laser with several kHz repetition rate should be utilized to obtain better tissue penetration and real time data acquisition.

This research was supported in part by the J. Crayton Pruitt Family Endowment. We thank Lijun Ji for help on histological sections.

[1]F. Helmchen and W. Denk, Nat. Methods **2**(12), 932 (2005).
[2]R. Yuste, Nat. Methods **2**(12), 902 (2005).
[3]D. Huang, E. Swanson, C. Lin, J. Schuman, W. Stinson, W. Chang, M. Hee, T. Flotte, K. Gregory, C. Puliafito, and J. Fujimoto, Science **254**(5035), 1178 (1991).
[4]C. Vinegoni, C. Pitsouli, D. Razansky, N. Perrimon, and V. Ntziachristos, Nat Methods **5**(1), 45 (2008).
[5]Y. Tan, M. Novo, L. Yao, L. Zhou, and H. Jiang, Mol. Imaging Biol. **13**(5), 868 (2011).
[6]D. Razansky, M. Distel, C. Vinegon, R. Ma, N. Perrimon, R. Köster, and V. Ntziachristos, Nat. Photonics **3**, 412 (2009).
[7]P. Beard, Interface Focus **1**, 602 (2011).
[8]S. Oladipupo, S. Hu, A. Santeford, J. Yao, J. Kovalski, R. Shohet, K. Maslov, L. Wang, and J. Arbeit, Blood **117**(15), 4142 (2011).
[9]T. Erpelding, C. Kim, M. Pramanik, L. Jankovic, K. Maslov, Z. Guo, J. Margenthaler, M. Pashley, and L. Wang, Radiology **256**(1), 102–110 (2010).
[10]S. Manohar, A. Kharine, J. C. G. van Hespen, W. Steenbergen, and T. G. van Leeuwen, J. Biomed. Opt. **9**(6), 1172 (2004).
[11]R. Kruger, R. Lam, D. Reinecke, S. Del Rio, and R. Doyle, Med. Phys. **37**(11), 6096 (2011).
[12]L. Xi, J. Sun, Y. Zhu, L. Wu, H. Xie, and H. Jiang, Biomed. Opt. Express **1**(5), 1278 (2010).
[13]L. Xi, S. Grobmyer, L. Wu, R. Chen, G. Zhou, L. Gutwein, J. Sun, W. Liao, Q. Zhou, H. Xie, and H. Jiang, Opt. Express **20**(8), 8726 (2012).
[14]Y. Yuan, S. Yang, and D. Xing, Appl. Phys. Lett. **100**, 023702 (2012).
[15]M. Li, H. Zhang, K. Maslov, G. Stoica, and L. Wang, Opt. Lett. **31**(4), 474 (2006).